Interpolating Scan and Oblique-Angle Tomograms in Myocardial PET Using Nitrogen-13 Ammonia

Michio Senda, Yoshiharu Yonekura, Nagara Tamaki, Hideo Saji, Harutoshi Koide, Ryuji Nohara, Hirofumi Kambara, Yutaka Konishi, and Kanji Torizuka

Department of Nuclear Medicine, Internal Medicine and Cardiovascular Surgery, Kyoto University School of Medicine, Kyoto, Japan

The effect of low sensitivity areas or gaps between adjacent slices of the multislice positron emission tomography on detection of myocardial perfusion abnormality with $^{13}NH_3$ was evaluated segmentally in 36 patients with coronary artery disease at rest or during exercise. The detectability of the defects in RCA or LAD region was 80% in single-position scans in stress studies. The false-negative defects were located mainly in the inferior wall, apicoinferior wall, or high anterior wall. When the patients were moved half the slice interval to perform the interpolating scan, and the two sets of images were interlaced with each other, the detectability increased to 88%. The interpolating scan also allowed reconstruction of long-axis and short-axis tomograms in high quality, which further improved the detectability of perfusion defects (100% for RCA or LAD and 75% for LCX lesion) and helped in understanding the anatomic relationships to the coronary artery territories.

J Nucl Med 27:1830–1836, 1986

Positron emission tomography (PET) provides superior sensitivity, resolution, and quantitative capability to single photon emission tomography (SPECT). We have found that myocardial perfusion PET images with nitrogen-13-labeled ammonia ($^{13}NH_3$) demonstrate a much higher quality than SPECT with thallium-201 (^{201}Tl) and that the PET images show homogeneous activity throughout the myocardium without fading in deep regions and can visualize fine structures such as papillary muscles and apical thinning (*1*). We have introduced stress myocardial perfusion studies with $^{13}NH_3$ and validated its clinical applicability to detect stenosed coronary vessels (*2*). Although the myocardial accumulation of $^{13}NH_3$ may not be determined solely by the regional blood flow (*3,4*), and, except for some preliminary investigations (*5*), a method for quantifying absolute regional flow needs yet to be established, imaging its relative distribution itself has an extensive clinical usefulness for diagnosis and treatment of patients with coronary artery disease (CAD) (*6–9*).

The axis of the heart, however, has an oblique angle to the long-axis of the body and transaxial tomograms alone may not provide sufficient information about the anatomic relationship of the coronary perfusion territories or for the observation of the inferior wall. Indeed, it is often advantageous to make long-axis or short-axis myocardial tomograms (*10*). The usefulness of such oblique-angle tomograms is well-established in SPECT with ^{201}Tl (*11*), but, to our knowledge, the attempt has never been reported in PET (*12*).

We have demonstrated that a low sensitivity area, or a gap, exists between adjacent slices in a multislice PET machine and that simple rebinning of the multislice transaxial PET images to make oblique-angle myocardial tomograms brings about considerable artifact (*13*). We have also introduced a new scanning method which we call the interpolating scan and have indicated its validity in filling up the gaps to allow reconstruction of high quality oblique-angle tomograms (*13*). The purpose of this study is to evaluate the clinical usefulness of the interpolating scan and the oblique-angle tomograms in detecting stenosed coronary arteries on rest or stress myocardial perfusion studies with $^{13}NH_3$ in patients with CAD.

MATERIALS AND METHODS

Preparation of [^{13}N]Ammonia

Nitrogen-13 ammonia was produced in a baby cyclotron* by bombarding water with protons involving the

Received Oct. 14, 1985; revision accepted Mar. 3, 1986.

For reprints contact: Michio Senda, MD, Dept. of Nuclear Medicine, Kyoto University School of Medicine, Shogoin, Sakyo-ku, Kyoto, 606 Japan.

^{16}O (p, α) ^{13}N nuclear reaction followed by reduction of oxides of ^{13}N with titanium trichloride and was obtained in a saline solution. The radiochemical purity of the product was >99.99%. The amount of activity administered in a clinical study ranged from 8 mCi to 20 mCi.

Tomographic Imaging

The instrument was a whole-body multislice positron computed tomograph, Positologica III, which provided seven slices of tomographic images at an interval of 16 mm (*14*). All studies were carried out in a nongated mode. The photon attenuation was corrected using the data of the transmission scan with an external source. The images were reconstructed with a Shepp-Logan filter convoluted with 2 mm sigma Gaussian. The spatial resolution was 9 mm FWHM at the center. The axial resolution was 12 mm FWHM at the center.

Because the slice pitch of Positologica III is 16 mm, which is not narrow enough compared with the axial resolution or myocardial thickness, simple rebinning of the multislice contiguous images obtained in a single-position scan to make long-axis or short-axis images would cause considerable artifacts. Therefore, following the first scan, the patient bed was moved half the slice interval in z-axis to carry out the so-called interpolating scan (*13*). After correcting for the variation of sensitivity among slices as well as decay and sampling time difference between the two scans, the two sets of seven contiguous images were interlaced with each other to make 8 mm-interval 14 contiguous images, from which the long-axis or short-axis tomograms were reconstructed. The spaces between the original slices were linearly interpolated. The pixel size of the final images was 4 mm.

Phantom Study

A phantom study was carried out to compare the capability of the transaxial images and the oblique-angle images to detect an inferior wall defect. A cone-shaped myocardial phantom simulating the human left ventricle was placed in the thoracic phantom simulating the human thorax (*15*). The "wall" of the left ventricle was 1-cm thick and a circular defect 1.5 cm in diameter was placed in the "inferior wall." The left ventricular wall was filled with a gallium-68 solution. Scans were performed in two different positions 8 mm apart and the long-axis and short-axis images were reconstructed.

The Effect of Attenuation Correction with Transmission Scan in a Slided Position

Since our protocol includes two scans at different positions, a transmission scan should be performed for each position if we want to correct the photon attenuation accurately. However, this would require another transmission scan which would increase the irradiation dose to the patient. In order to evaluate the effect of attenuation correction with inappropriately positioned transmission scan in a normal volunteer, myocardial perfusion images were reconstructed using the transmission scan performed at the correct position and then after moving 8 mm, and the images were compared.

Clinical Studies

The clinical material studied consisted of seven normal subjects and 23 patients with coronary artery diseases. The patients had a history of myocardial infarction (MI) or angina pectoris (AP) or both. Coronary angiography was performed in all patients to confirm diseased coronary arteries. A coronary branch with >50% stenosis was defined as a diseased vessel. Also, left ventriculography (LVG) was performed in each patient to evaluate segmental wall motion abnormalities.

Myocardial perfusion studies were performed at rest in 22 cases (six normal and 16 CAD patients) and during exercise in 25 cases (five normal and 20 CAD patients). Eighteen cases (four normal and 14 CAD patients) were studied both at rest and during exercise. All individuals gave written consent.

The subject was positioned in the gantry and the transmission scan was performed. In the stress study, the exercise was performed using a supine bicycle ergometer attached to the PET bed. A graded work load was started at 25W and increased by 25W every 3 min until the patient complained of fatigue or chest pain, the electrocardiogram showed significant ST segment depression, or the load reached 85% of maximum heart rate. The patient continued exercise for 30 sec after i.v. injection of $^{13}NH_3$. Whether in the resting or stress study, the first scan was carried out for a duration of 5 min beginning 3 min postinjection of $^{13}NH_3$ in a position 4 mm rostral to that of the transmission scan. This was followed by a second scan carried out for 8 min in a position 8 mm caudal to that of the first scan. The two sets of transaxial images and the oblique-angle tomograms were reconstructed as described above.

The images obtained were studied qualitatively by two independent observers with regard to the presence of low perfusion in each myocardial segment. The case was considered abnormal in the right coronary artery (RCA), left anterior descending artery (LAD), or left circumflex artery (LCX) when decreased tracer activity was observed in the inferior or posterior wall, anteroseptal or apical wall, or lateral wall, respectively (*2*). When there was a discrepancy between the two judges, the images were reviewed again for a consensus. The image analysis was carried out first using each of the 7-slice contiguous images, then using the interlaced 14-slice images, and finally using additional long-axis and short-axis images.

RESULTS

Phantom Study

In the myocardial phantom study, the defect was apparently not detected in the 14-slice transaxial con-

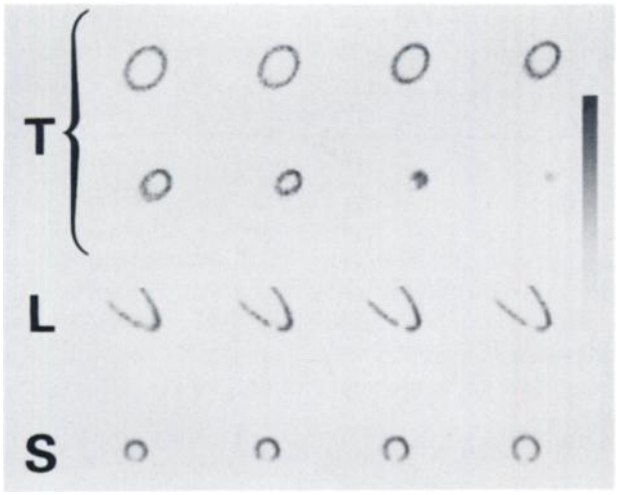

FIGURE 1
Transaxial (T), long-axis (L) and short-axis (S) tomograms of myocardial phantom with inferior defect of 1.5 cm diameter. Defect was not visualized in transaxial images at 8 mm interval, but was clearly delineated in long-axis and short-axis tomograms

tiguous images. However, the long-axis and the short-axis images clearly delineated the defect in the inferior wall (Fig. 1).

Effect of Attenuation Correction in Inappropriate Position

The transaxial emission images corrected for photon attenuation with the transmission scan carried out at correct and 8-mm slided position were compared. Both images showed similar appearance except for the activity in the liver dome (Fig. 2).

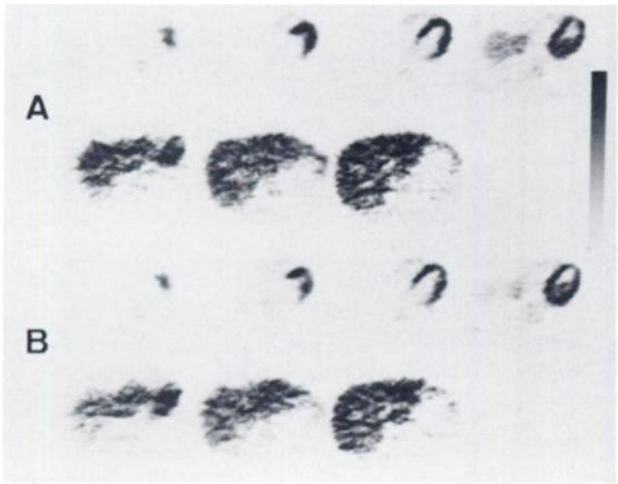

FIGURE 2
Contiguous transaxial myocardial tomograms with $^{13}NH_3$ of normal volunteer reconstructed with photon attenuation correction using transmission scan at correct position (A) and at 8 mm rostral position (B)

Clinical Studies

The images of the first scan were successfully interpolated with the second scan to make oblique-angle myocardial tomograms in 45 of the 47 studies. The remaining two cases showed a significant increase of activity during the two scans resulting in the failure of the three-dimensional reconstruction.

In all normal cases, no perfusion defect was observed in any segment in rest or exercise (specificity 100%).

Table 1 summarizes the results of the myocardial PET studies in 36 cases with CAD. Resting images revealed perfusion abnormality in 15 of 32 scans in single position (47%). The detectability was 50% when interpolating scan was combined, and increased to 69% when oblique-angle images were added to the material. In stress studies, the detectability was 83% in single position scan, but increased to 90% by interpolation and to 100% when oblique-angle images were utilized. Table 2 shows the results of the segmental analysis. Detectability of RCA or LAD involvement was improved by the interpolating scan and further by the oblique-angle tomograms while less improvement was observed in patients with LCX disease. No perfusion defect was observed in any segment without stenosis of the corresponding coronary artery. Perfusion defects in which the interpolating scan or the oblique-angle tomograms were needed for detection included those in the inferior (RCA disease), apicoinferior (LAD disease) or high anterior wall (LAD disease). Table 3 shows how the presence of wall motion abnormality affects the detectability in rest studies. When the diseased arteries were confined to those with wall motion abnormality of the corresponding segments the detectability was improved significantly. On the other hand, only three out of 11 diseased segments without wall motion abnormality showed perfusion defects in oblique-angle tomograms.

Figures 3, 4, and 5 represent three typical cases in which interpolating scan and oblique-angle tomograms were particularly useful to detect perfusion abnormality. Figure 3 shows a case with RCA involvement. The transaxial tomograms showed no perfusion defects whereas the long-axis and short-axis tomograms clearly

TABLE 1
Detectability of Coronary Artery Disease

	Resting	Stress
Single-position scan	15/32 (47%)	33/40 (83%)
First scan	8/16	16/20
Second scan	7/16	17/20
Interpolated transaxial	8/16 (50%)	18/20 (90%)
Additional oblique-angle	11/16 (69%)	20/20 (100%)

TABLE 2
Detectability of Individual Coronary Artery Involvement

	Resting				Stress			
	RCA	LAD	LCX	Total	RCA	LAD	LCX	Total
Single-position scan	10/16 (63%)	11/28 (39%)	9/18 (50%)	30/62 (48%)	8/14 (57%)	32/36 (89%)	10/16 (63%)	50/66 (76%)
First scan	5/8	5/14	5/9	15/31	5/7	15/18	6/8	26/33
Second scan	5/8	6/14	4/9	15/31	3/7	17/18	4/8	24/33
Interpolated transaxial	6/8 (75%)	7/14 (50%)	5/9 (56%)	18/31 (58%)	5/7 (71%)	17/18 (94%)	6/8 (75%)	28/33 (85%)
Additional oblique-angle	8/8 (100%)	9/14 (64%)	5/9 (56%)	22/31 (71%)	7/7 (100%)	18/18 (100%)	6/8 (75%)	31/33 (94%)

indicated perfusion defects in the posterior and inferior wall. Figure 4 shows a case with anterior small MI. The transaxial tomograms had difficulty in detecting a perfusion defect in the high anterior wall, which was clearly observed in the long-axis tomograms. Figure 5 shows a case with effort angina involving LAD. The stress study indicated no more perfusion abnormality than an apical thinning in the transaxial tomograms but an apparent defect was observed in the apicoinferior wall in the long-axis tomograms.

DISCUSSION

The axial point spread function of a multislice PET machine is approximately a triangle at or near the center of the field-of-view, and the sensitivity for any slice decreases significantly as the source moves away from the middle of the slice thickness. Accordingly there are low sensitivity regions or gaps between adjacent slices in a multislice PET machine. Although their width depends on the geometry of the scanner, these gaps occur in most PET scanners as long as some spacing exists between adjacent detector rings. These invisible regions are particularly significant when the object is thin enough in z-axis, and the so-called interpolating scan is valuable to fill up the gaps (*13*).

Our results indicated that the detectability of CAD as a myocardial perfusion defect in stress $^{13}NH_3$ PET images increased from 83% to 90% when the interpolating scan was utilized. In the segmental analysis, the interpolating scan helped the detectability increase from 57% to 71% in RCA disease and from 89% to 94% in LAD disease. On the other hand the detectability of LAD disease was less improved. The resting studies showed similar tendency. The single-position scans had difficulty in detecting those small defects located in the inferior (RCA), apicoinferior (LAD), or high anterior wall (LAD). The myocardial walls in those particular regions are almost vertical to the z-axis and may drop into the gaps in single-position scans. These results indicate that the gaps between adjacent slices in a multislice PET are significant in clinical application and that the single-position scanning may induce some false-negative results in myocardial perfusion studies in cases with small perfusion defects within the segments vertical to the z-axis. The interpolating scan was useful to detect those defects and to improve the sensitivity without decreasing the specificity.

It has been pointed out that the axis of the heart has an oblique angle to the long-axis of the body and that the transaxial tomograms alone may not be sufficient to understand the anatomic relationship to the coronary artery territories. SPECT with rotating gamma camera has a fine z-axis sampling allowing the three-dimensional reconstruction to make long-axis or short-axis myocardial tomograms with ^{201}Tl, and the usefulness of these oblique-angle tomograms is well-established

TABLE 3
Detectability of Individual Coronary Artery Involvement in Resting Studies Classified by Corresponding Segmental Wall Motion Abnormalities Observed in Left Ventriculography

	With wall motion abnormality				Without wall motion abnormality			
	RCA	LAD	LCX	Total	RCA	LAD	LCX	Total
Single-position scan	9/12 (75%)	11/20 (55%)	7/8 (88%)	27/40 (68%)	1/4	0/8	2/10	3/22 (14%)
First scan	5/6	5/10	4/4	14/20	0/2	0/4	1/5	1/11
Second scan	4/6	6/10	3/4	13/20	1/2	0/4	1/5	2/11
Interpolated transaxial	5/6 (83%)	7/10 (70%)	4/4 (100%)	16/20 (80%)	1/2	0/4	1/5	2/11 (18%)
Additional oblique-angle	6/6 (100%)	9/10 (90%)	4/4 (100%)	19/20 (95%)	1/2	1/4	1/5	3/11 (27%)

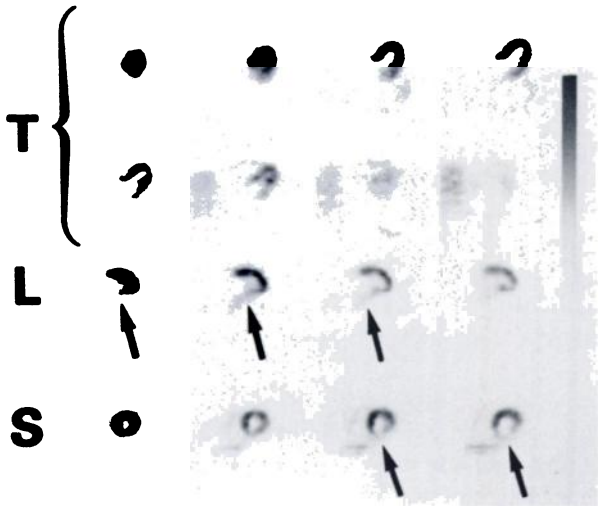

FIGURE 3
Stress myocardial tomograms with $^{13}NH_3$ of patient with RCA disease. Transaxial tomograms (T) could not detect perfusion defect in inferior wall, which was easily detected in long-axis (L) or short-axis (S) images (arrows)

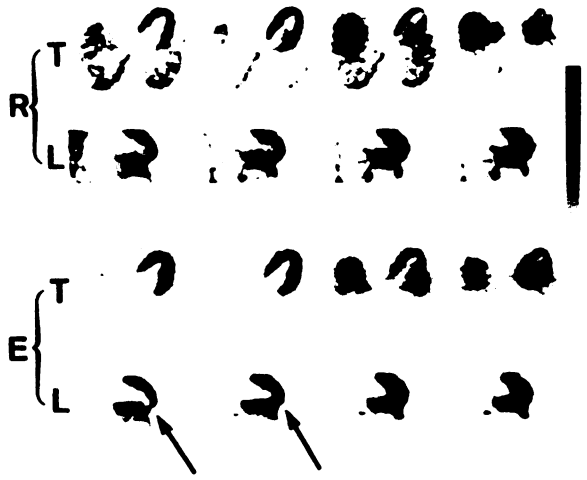

FIGURE 5
Transaxial (T) and long-axis (L) myocardial perfusion tomograms of patient with effort angina involving LAD in rest (R) and stress (S) studies. Rest images as well as stress transaxial images showed no more perfusion abnormality than apical thinning, while stress long-axis images revealed a defect in apicoinferior wall (arrows). Rest images confirm that stress, and not artifact or apical thinning, induced apparent defect in stress long-axis images

(*10,11*). However, the z-axis sampling of PET is insufficient to allow three-dimensional reconstruction and the attempt has not yet been made. We have introduced a new scanning method, interpolating scan, which has filled up the gaps between slices and allowed oblique-angle myocardial tomograms of high quality to be made (*13*).

The results of our phantom study indicated that an inferior defect in the myocardial phantom was difficult to detect in the transaxial tomograms but was easily detected in the oblique-angle tomograms. Our clinical studies indicated that some perfusion defects in the inferior (RCA region), apicoinferior or high anterior wall (LAD region) were difficult to detect with the interpolated transaxial tomograms but were easily detected with oblique-angle tomograms. The detectability was increased from 71% to 100% in RCA cases and from 94% to 100% in LAD cases in stress perfusion studies. The transaxial tomograms have the same digital information as the oblique-angle tomograms, and they should be equivalent for a "computer's eye." The abovementioned segments to a human observer, however, are nearly tangential to the image plane in transaxial images with the heart wall appearing as a mass rather than a ring, and the decreased activity in those segments does not contrast well with the other regions in a single transaxial image, resulting in the failure of detecting the perfusion defects. The oblique-angle tomograms not only improved the sensitivity to detect the perfusion abnormality without decreasing the specificity but also helped understand the anatomic extension of the diseased area.

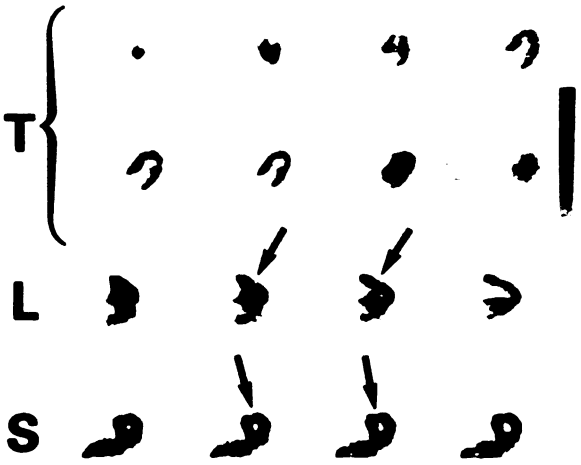

FIGURE 4
Resting myocardial perfusion images of patient with anterior wall old myocardial infarction. He has history of chest pain and electrocardiogram suggested anterior wall MI. Obstruction of branch of LAD was observed in CAD. Transaxial tomograms (T) could only detect unequivocal low perfusion in high anterior wall, which was easily detected in long-axis (L) or short-axis (S) images (arrows)

Depending on the degree of obstruction, and also owing to the presence of collateral circulations, the regional myocardial perfusion in the resting state is not simply determined by the patency of the coronary artery supplying that region. Our results indicated that only 71% of total diseased segments were detected in combined transaxial and oblique-angle images in resting studies (Table 2). The perfusion may be preserved at

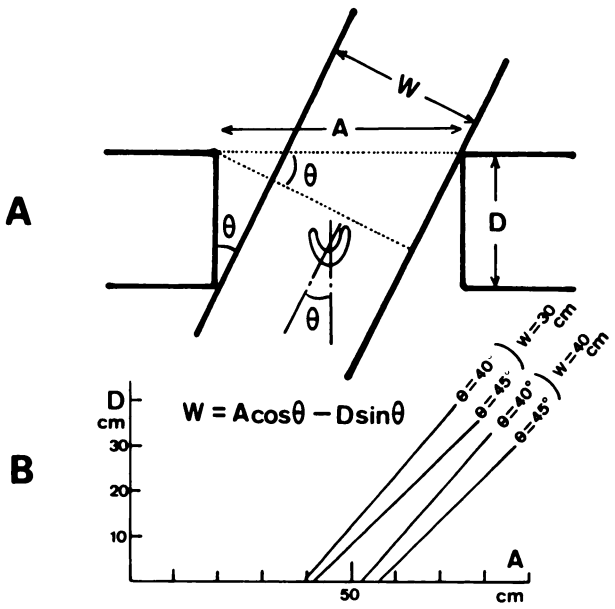

FIGURE 6

Possibility of direct acquisition of short axis views by tilting gantry and/or bed. A: If aperture of gantry has cylindrical form, relationship of $W = A\cos\theta - D\sin\theta$ holds, where W is maximum possible thickness of patient body (plus bed) measured within plane defined by cardiac axis and body axis, A and D are aperture diameter and depth of the gantry, and θ is angle between bed and gantry axis which is geometric sum of vertical and lateral tilting angles. When axis of heart is 45° apart from long axis of body, θ should be 45° for direct short-axis scan. Depth D includes thickness of lead shield and accompanying mechanics and is usually far larger than axial field-of-view. B: Graphic expression of above relationship. For example, when D = 20 cm, A = 76 cm, and θ = 45°, body must be thinner than 30 cm

least in some segments of the residual 29%. In fact when the diseased segments were confined to those with segmental wall motion abnormality proved in LVG, the detectability increased significantly (95%, Table 3). Although wall motion abnormality in CAD does not always reflect regional hypoperfusion, this would in some way support the above hypothesis. On the other hand, three out of 11 diseased segments without wall motion abnormality showed perfusion defects in combined transaxial and oblique-angle tomograms (Table 3). These three defects are considered to be either artifacts (false-positive defects) or true defects too small to induce wall motion abnormality.

Some PET scanners may allow vertical and lateral tiltings of the imaging gantry (or the patient bed), and one would think that short-axis views could easily be acquired directly; however, this is not the case. The possibility of direct short-axis scan depends not only on the tilting capability, but also on the depth and aperture of the gantry. Figure 6 represents the relationship of those parameters. The angle between the cardiac axis and the body axis can be estimated, for example, by right anterior oblique roentogenogram. When this angle is 45°, the gantry should be tilted relatively 45° to the bed to acquire short-axis views of the heart. In that case, for a scanner 76 cm wide and 20 cm deep, for example, the body must be thinner than 30 cm. Thus, a scanner with extremely thin or wide gantry must be prepared for direct acquisition of the short-axis views. And in that special case as well, invisible regions would exist between consecutive slices of the short-axis images.

In order to make a three-dimensional reconstruction using an interpolating scan the activity should not change during the two scans. Earlier we reported gradual increases in activity in normal segments and less increases in infarcted segments in serial 5-min dynamic studies for 30 min (*16*). Regional myocardial activity is not directly the regional myocardial blood flow. Actually, the regional activity in the first scan is a complex function of blood flow and other physiological parameters and that of the second scan is another complex function of them (*3,4*). Combining these two sets of images to make oblique-angle tomograms would make something like a "chimera" image with some pixels representing some aspects of the regional myocardial physiology and other pixels representing other aspects. Qualitatively, however, oblique angle images were successfully reconstructed in 45 of 47 cases (96%), which were extremely useful as discussed above. Thus the "chimera" effects are considered to be less harmful than inadequate z-axis sampling. If the method of obtaining the absolute value of the regional myocardial blood flow to make functional images (flow images) is established using $^{13}NH_3$ or other more suitable tracers (*5, 17*), it is recommended to use those functional images for three-dimensional reconstruction rather than the gross original images.

Our results indicated that one transmission scan was sufficient to correct for photon attenuation in two-emission scans in an 8-mm slided position. This helped diminish the duration of study and the radiation dose.

Our method can be applied to other PET studies using other positron-emitting tracers which could evaluate various aspects of the myocardial performance including the glucose metabolism and fatty acid metabolism (*9,18–20*). The interpolating scan and the oblique-angle tomograms should be useful for the detection of hot or cold segments and the understanding of the anatomic relations of these studies as well.

FOOTNOTE

*CYPRIS, Model 325, Sumitomo, Tokyo, Japan.

REFERENCES

1. Tamaki N, Yonekura Y, Senda M, et al: Comparative study of myocardial perfusion imaging by Tl-201 sin-

gle photon ECT and N-13 ammonia positron CT. *J Nucl Med* 25:P6, 1984 (abstr)
2. Tamaki N, Yonekura Y, Senda M, et al: Myocardial positron computed tomography with N-13 ammonia at rest and during exercise. *Eur J Nucl Med* 11:246–251, 1985
3. Bergmann SR, Hack S, Tewson T, et al: The dependence of accumulation of $^{13}NH_3$ by myocardium on metabolic factors and its implication for quantitative assessment of perfusion. *Circulation* 61:34–43, 1980
4. Rauch R, Helus F, Grunze M, et al: Kinetics of ^{13}N-ammonia uptake in myocardial cells indicating potential limitations in its applicability as a marker of myocardial blood flow. *Circulation* 71:387–393, 1985
5. Shah A, Schelbert HR, Schwaiger M, et al: Measurement of regional blood flow with N-13 ammonia and positron-emission tomography in intact dogs. *J Am Coll Cardiol* 5:92–100, 1985
6. Schelbert HR, Phelps ME, Hoffman EJ, et al: Regional myocardial perfusion assessed with N-13 labeled ammonia and positron emission computerized axial tomography. *Am J Cardiol* 43:209–218, 1979
7. Gould KL, Schelbert HR, Phelps ME, et al: Noninvasive assessment of coronary stenoses with myocardial perfusion imaging during pharmacologic coronary vasodilation. V. Detection of 47 percent diameter coronary stenosis with intravenous nitrogen ammonia and emission-computed tomography in intact dogs. *Am J Cardiol* 43:200–208, 1979
8. Schelbert HR, Wisenberg G, Phelps ME, et al: Noninvasive assessment of coronary stenoses by myocardial imaging during pharmacologic coronary vasodilation. VI. Detection of coronary artery disease in human beings with intravenous N-13 ammonia and positron computed tomography. *Am J Cardiol* 49:1197–1207, 1982
9. Marshall RC, Tillisch JH, Phelps ME, et al: Identification and differentiation of resting myocardial ischemia and infarction in man with positron computed tomography, ^{18}F-labeled fluorodeoxyglucose and N-13 ammonia. *Circulation* 67:766–778, 1983
10. Borrello JA, Clinthorne NH, Rogers L, et al: Oblique-angle tomography: A restructuring algorithm for transaxial tomographic data. *J Nucl Med* 22:471–473, 1981
11. Tamaki N, Yonekura Y, Mukai T, et al: Segmental analysis of stress thallium myocardial emission tomography for localization of coronary artery disease. *Eur J Nucl Med* 9:99–105, 1984
12. Ter-Pogossian MM, Mullani NA, Hood J, et al: A multislice positron emission computed tomograph (PETT IV) yielding transverse and longitudinal images. *Radiology* 128:477–484, 1978
13. Senda M, Yonekura Y, Tamaki N, et al: Axial resolution and the value of interpolating scan in multislice positron computed tomography. *IEEE Trans Med Imag* MI-4:44–51, 1985
14. Senda M, Tamaki N, Yonekura Y, et al: Performance characteristics of Positologica III: A newly designed whole-body multislice positron computed tomograph. *J Comp Assist Tomogr* 9:940–946, 1985
15. Tamaki N: T1-201 single-photon emission computed tomography (SPECT) (reply). *J Nucl Med* 24:274–275, 1983
16. Tamaki N, Senda M, Yonekura Y, et al: Dynamic positron computed tomography of the heart with a high sensitivity positron camera and nitrogen-13 ammonia. *J Nucl Med* 26:567–574,1985
17. Huang SC, Schwaiger M, Carson RE, et al: Quantitative measurement of myocardial blood flow with oxygen-15 water and positron computed tomography: An assessment of potential and problems. *J Nucl Med* 26:616–625, 1985
18. Schoen HR, Schelbert HR, Robinson G, et al: C-11 labeled palmitic acid for the noninvasive evaluation of regional myocardial fatty acid metabolism with positron-computed tomography. I. Kinetics of C-11 palmitic acid in normal myocardium. *Am Heart J* 103:532–547, 1982
19. Schoen HR, Schelbert HR, Najafi A, et al: C-11 labeled palmitic acid for the noninvasive evaluation of regional myocardial fatty acid metabolism with positron-computed tomography. II. Kinetics of C-11 palmitic acid in acutely ischemic myocardium. *Am Heart J* 103:548–561, 1982
20. Lerch RA, Bergmann SR, Ambos HD, et al: Effect of flow-independent reduction of metabolism on regional myocardial clearance of ^{11}C-palmitate. *Circulation* 65:731–738, 1982